Stagnation-Point Heat Transfer During Impingement of Laminar Liquid Jets: Analysis Including Surface Tension

Xin Liu[1]

L. A. Gabour
Graduate Student.

J. H. Lienhard V
Associate Professor.

Department of Mechanical Engineering,
Massachusetts Institute of Technology,
Cambridge, MA 02139

The stagnation-zone characteristics of an impinging liquid jet are of great interest because the maximum heat transfer coefficient occurs in that region. This paper is an analytical study of the fluid flow and heat transfer in the stagnation zone of an unsubmerged liquid jet. The role of surface tension is emphasized. Stagnation-zone transport is strongly dependent on the potential flow above the boundary layer. Only a few studies have examined the potential flow of an unsubmerged jet, each using approximate potential flow theory and neglecting surface tension. In this paper, numerical solutions for a laminar unsubmerged jet are obtained, using a simulation method for steady, inviscid, incompressible flow with surface tension. A series solution that satisfies the boundary conditions in an approximate manner is constructed in terms of Legendre functions. Numerical solution of the momentum equation shows that surface tension has an effect on the stagnation-point flow field when the Weber number is small. Solutions of the associated boundary layer problem are used to obtain predictions of the influence of Weber number on the stagnation-zone heat transfer. The results are validated by comparison to measurements at high Weber number.

1 Introduction

The stagnation zone of an impinging jet is characterized by an extremely thin thermal boundary layer. This results in a very large heat transfer coefficient, but it also sensitizes the stagnation-zone cooling efficiency to various parametric influences that would be less important for a thicker thermal boundary layer. Such effects include minor variations in the free-stream flow field, wall roughness, wall conduction, and so on. In this paper, we examine the role of surface tension, which can change the shape of the jet's free surface and alter the radial velocity gradient over the stagnation-zone boundary layer.

The stagnation-point flow field has been studied extensively for submerged jets. The theory is based on an infinite flow field assumption under which the partial differential equations of the boundary layer admit a similarity transformation (Schlichting, 1979; White, 1991). The free-stream flow is determined from a separate potential-flow calculation. For an unsubmerged jet, the free surface between the liquid and gas phases imposes an additional boundary condition, which greatly complicates the calculation of the inviscid flow above the wall boundary layer; a numerical solution is required. The influence of the free surface on the near-wall flow field is even more complex for small Weber numbers, when surface tension effects are strong. This may be of particular concern for small-diameter jets.

Numerical methods for free-surface problems generally fall into one of two classes (Crank, 1984). In the first class, the problem is solved as originally formulated in the physical plane. After computation of approximate trial solutions, the free boundary is adjusted numerically to an improved free boundary. In the second class, the problem is recast by some suitable change of coordinates, and the transformed problem is solved numerically as a fixed-boundary problem.

To avoid solving the full Navier–Stokes equations, the stagnation flow can be divided into an inviscid flow and a boundary layer. The inviscid flow, which provides the free-stream condition needed for the near-wall viscous flow, represents the primary computational problem. Schach (1935) employed an integral-equation method, which was developed from Green's theorem. Shen (1962) expanded the velocity potential in a series using Legendre polynomials. The free-streamline boundary condition was satisfied in an average manner. Shen suggested an iteration scheme, but it lacked a method for successively correcting the approximated free-streamline position and it was not actually carried out. Strand (1964) expanded the velocity potential in Bessel functions. The free-streamline boundary condition was satisfied by discrete points. None of those solutions included the surface tension.

In the following, a series solution that includes surface tension is constructed. An iteration scheme for the free surface is conducted using a correction function. The solution is given by Legendre functions and satisfies the free-surface boundary conditions in an approximate manner, with accuracy improving as more terms are retained. The solution is validated by comparison to experimental data for high Weber number, laminar jets, which have both uniform velocity profiles and large Reynolds numbers.

2 Analysis

The flow field is separated into an outer, inviscid, irrotational flow and a near-wall viscous boundary layer. The inviscid flow is determined using potential-flow theory with surface tension along the free streamline. The resulting radial velocity distribution along the wall is used as the free-stream flow in the subsequent boundary-layer calculation. Gravitational effects are neglected.

Inviscid Impinging Jet Flow. For an inviscid, axisymmetric, and irrotational jet (Fig. 1), the velocity potential is given by

$$\nabla^2\phi = 0 \tag{1}$$

[1] Present address: Carrier Corporation, Syracuse, NY.

Contributed by the Heat Transfer Division for publication in the JOURNAL OF HEAT TRANSFER. Manuscript received by the Heat Transfer Division April 3, 1992; revision received June 26, 1992. Keywords: Forced Convection, Jets. Associate Technical Editor: F. P. Incropera.

Copyright © 1993 by ASME
Downloaded 29 Jun 2009 to 18.80.1.33. Redistribution subject to ASME license or copyright; see http://www.asme.org/terms/Terms_Use.cfm

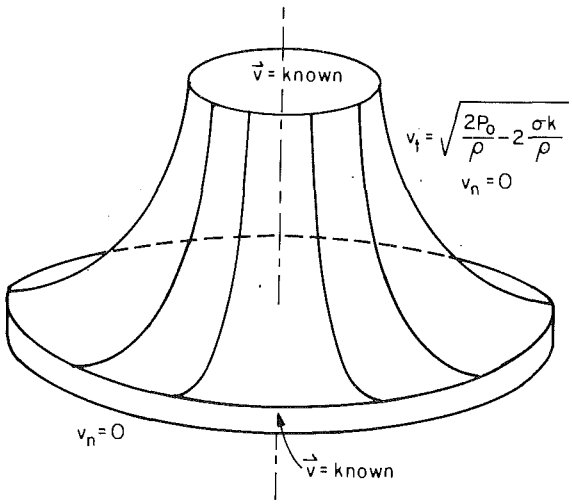

Fig. 1 Computational domain and boundary conditions

The boundary condition along the inlet to the computational domain is

$$\mathbf{v} = \text{known} = \mathbf{u}_f \tag{2}$$

In the present computation, the inlet velocity is assumed to be uniform (and thus irrotational) and purely downward. The inlet is located at a distance of one diameter above the wall; the orifice producing the jet is presumably somewhat farther above the wall. For a jet issuing from a plenum, the influence of surface tension on the inlet velocity must be taken into account as

$$u_f = C_v\sqrt{\frac{2P_0}{\rho}} = \sqrt{1-\frac{4}{\mathrm{We}_d}}\sqrt{\frac{2P_0}{\rho}} \tag{3}$$

for sharp-edged orifices, with C_v the velocity coefficient, P_0 the plenum gage pressure, ρ the liquid density, and We_d the Weber number.[2] The Weber number characterizes the magnitude of the surface tension pressure relative to the dynamic pressure:

$$\mathrm{We}_d = \frac{\rho u_f^2 d}{\sigma} \tag{4}$$

where σ is the surface tension and d is the jet diameter.

Along the free streamline, the velocity normal to the surface is obtained from the condition of no flow through the liquid surface:

$$v_n = 0 \tag{5}$$

The velocity tangent to the streamline is obtained from Bernoulli's equation:

$$v_t = \sqrt{\frac{2P_0}{\rho} - 2\frac{\sigma\kappa}{\rho}} \tag{6}$$

where κ is the curvature of the free surface. The Bernoulli constant is evaluated at the inlet and has the same value for all streamlines. Along the target plate and the axis of symmetry

$$v_n = 0 \tag{7}$$

[2] Lienhard and Lienhard (1984) showed viscous losses to have a negligible effect on C_v for a sharp-edged orifice. Equation (3) above corrects an error in their handling of surface tension for a circular jet's C_v. The correct expression for C_v is $\sqrt{1 - K_2 C_D^{3/2}/\sqrt{\mathrm{Re}_d} - 4/\mathrm{We}_d}$ for $K_2 = 0.242738$ and C_D the discharge coefficient ($\simeq 0.611$). Equation (3) is correct to ~ 0.1 percent for $\mathrm{We}_d \geq 10$ and $\mathrm{Re}_d \geq 10000$.

Nomenclature

A_0, A_1, A_2 = consts in Eq. (25)
A_{2n} = consts in Eq. (20)
B = dimensionless velocity gradient $= 2(d/u_f)(\partial U/\partial r)$
B_n = consts in Eq. (25)
C_n = consts in Eq. (25)
C_v = velocity coefficient for liquid jets
d = jet diameter, fully contracted, m
d_o = orifice diameter, m
$f_n(\theta)$ = any continuous function of θ
h = heat transfer coefficient $= q_w/(T_w - T_f)$, W/m^2 K
$G(\mathrm{Pr})$ = function of Prandtl number given by Eq. (31)
k = thermal conductivity of liquid, W/m K
Nu_d = Nusselt number based on jet diameter $= q_w d/k(T_w - T_f)$
p = local gage pressure in liquid, Pa
P_0 = gage pressure in plenum, Pa
P_{2n} = Legendre function of $2n$ order
Pr = Prandtl number of liquid
Q = volume flow rate of jet, m^3/s
q_w = wall heat flux, W/m^2
r = radius coordinate in spherical coordinates, or radius coordinate in cylindrical coordinates, m
$R(\theta)$ = spherical radius-coordinate of free surface, m
Re_d = Reynolds number of the jet $= u_f d/\nu$
T_w, T_f = temperature of wall, incoming liquid jet, K
u, v = liquid velocity components in radial, axial direction of cylindrical coordinates, m/s
u_f = incoming jet velocity $= C_v\sqrt{2P_0/\rho}$, m/s
$U(r)$ = radial velocity just outside boundary layer, m/s
$\mathbf{v}$ = liquid velocity vector $= \nabla\phi$, m/s
v_n = normal velocity in streamline coordinates, m/s
v_t = tangent velocity in streamline coordinates, m/s
We_d = Weber number $= \rho u_f^2 d/\sigma$
y = axial coordinate in cylindrical coordinates, m
α = thermal diffusivity of liquid, m^2/s
β = numerical relaxation factor
θ = polar angle of spherical coordinates
κ = free surface curvature, m^{-1}
μ = dynamic viscosity of liquid, kg/m s
ν = kinematic viscosity of liquid, m^2/s
ρ = density of liquid, kg/m^3
σ = surface tension, N/m
ϕ = velocity potential, m^2/s
$\partial/\partial n$ = derivative normal to the solution domain boundary
$\partial/\partial t$ = derivative tangent to the solution domain boundary

Superscripts

(n) = result from the nth iteration
$*$ = dimensionless variable

Downloaded 29 Jun 2009 to 18.80.1.33. Redistribution subject to ASME license or copyright; see http://www.asme.org/terms/Terms_Use.cfm

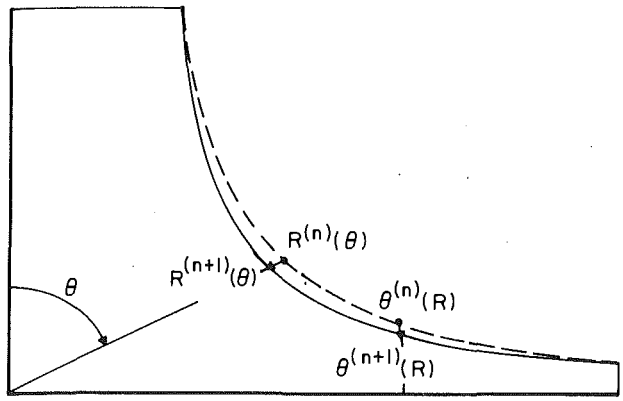

Fig. 2 Free-surface iteration

Schach's results (1935) show that the velocity is essentially uniform and parallel to the target plate for a radius larger than 1.25 diameter. In the present computation, the outlet is placed at $r/d = 1.25$ and the outlet velocity is assumed uniform and parallel to the target. From Bernoulli's equation, the outlet speed is then

$$v_t = \sqrt{\frac{2P_0}{\rho}} \tag{8}$$

neglecting the free surface curvature.

Inlet Velocity Profile Boundary Condition. Our calculations assume a uniform velocity distribution for the incoming jet. This distribution occurs, for example, at a few diameters distance from a sharp-edged orifice. Often, the velocity profiles of jets issuing from nozzles are not uniform. A jet flowing from a long pipe, in which the flow is fully developed, has a parabolic velocity profile if it is laminar or a one-seventh power law profile if it is turbulent. Other cases may lie between these nonuniform distributions. However, for long jets, viscosity (or turbulent mixing) will produce a uniform profile at large distances from the nozzle.

Previous investigations have shown that a nonuniform velocity profile can produce larger stagnation-point velocity gradients and higher Nusselt numbers than for a uniform profile. For example, prediction and experiments by Scholtz and Trass (1970) showed that an axisymmetric, parabolic profile jet has 2.27 times the heat transfer of a uniform-profile jet. Sparrow and Lee (1975) found similar results for planar jets. Previous studies also show that velocity profile effects become more pronounced as the nozzle is moved very close to the target ($l/d < 1$). Furthermore, many experimental and numerical studies show that the distance at which the surface velocity approaches the mean velocity depends strongly on both the nozzle type and Reynolds number (Scriven and Pigford, 1959; Duda and Vrentas, 1967; Davies and Makepeace, 1978).

The Physical Coordinates and Nondimensional Equations. If Eqs. (1)–(8) are to be solved, a choice of a physical coordinate system is required. Cylindrical coordinates (Strand, 1964) have the advantage that the boundary conditions at the inlet and outlet are simplified, since the inlet and outlet coincide with one of the coordinate planes. However, concurrent difficulties occur because the free-surface derivatives in these coordinates become either infinite or zero at the inlet and outlet. While those derivatives are irrelevant for the zero-surface-tension case, they are essential when surface tension is included. Spherical coordinates (Shen, 1962) avoid the above problems while preserving the simplicity of the mathematical expressions. We adopt spherical coordinates with radius r and polar angle θ. The origin is placed at the stagnation point with the pole along the vertical axis of symmetry; the free-surface radius is $R(\theta)$ (Fig. 2).

Dimensionless velocity is defined relative to the ideal-jet velocity:

$$\mathbf{v}^* = \frac{\mathbf{v}}{u_f} \tag{9}$$

The coordinates r and R are nondimensionalized as

$$r^* = \frac{r}{2d} \tag{10}$$

$$R^* = \frac{R}{2d} \tag{11}$$

The factor of 2 is included to make the dimensionless radius less than unity in the computational domain so as to guarantee the convergence of the series expansion (Eq. (20)). In addition, we scale the velocity potential and the surface curvature as

$$\phi^* = \frac{\phi}{2du_f} \tag{12}$$

$$\kappa^* = 2d\kappa \tag{13}$$

In terms of the velocity potential, the dimensionless equation of motion is

$$\nabla^2\phi^* = \left[\frac{1}{r^{*2}}\frac{\partial}{\partial r^*}\left(r^{*2}\frac{\partial}{\partial r^*}\right) + \frac{1}{r^{*2}\sin\theta}\left(\frac{\partial}{\partial\theta}\sin\theta\frac{\partial}{\partial\theta}\right)\right]\phi^* = 0 \tag{14}$$

The boundary condition along the inlet (Eqs. (2)–(3)) is

$$\left(\frac{\partial\phi^*}{\partial n^*}\right)_{\text{inlet}} = \frac{\partial\phi^*}{\partial r^*}\cos\theta - \frac{1}{r^*}\frac{\partial\phi^*}{\partial\theta}\sin\theta = -1 \tag{15}$$

The boundary condition along the outlet (Eq. (8)) is

$$\left(\frac{\partial\phi^*}{\partial n^*}\right)_{\text{outlet}} = \frac{\partial\phi^*}{\partial r^*}\sin\theta + \frac{1}{r^*}\frac{\partial\phi^*}{\partial\theta}\cos\theta = \sqrt{1+4/\text{We}_d} \tag{16}$$

Along the free surface, the boundary conditions (Eqs. (5)–(6)) are

$$\left(\frac{\partial\phi^*}{\partial n^*}\right) = \frac{1}{\sqrt{\left(\frac{1}{R^*}\frac{dR^*}{d\theta}\right)^2+1}}\left(\frac{\partial\phi^*}{\partial r^*} - \frac{1}{r^{*2}}\frac{\partial\phi^*}{\partial\theta}\frac{dR^*}{d\theta}\right) = 0 \tag{17}$$

$$\left(\frac{\partial\phi^*}{\partial t^*}\right) = \frac{1}{\sqrt{\left(\frac{1}{R^*}\frac{dR^*}{d\theta}\right)^2+1}}\left(\frac{1}{r^*}\frac{\partial\phi^*}{\partial r^*}\frac{dR^*}{d\theta} + \frac{1}{r^*}\frac{\partial\phi^*}{\partial\theta}\right) = \sqrt{1-\kappa^*/\text{We}_d+4/\text{We}_d} \tag{18}$$

The dimensionless curvature of the free surface, κ^*, is given by:

$$\kappa^* = \frac{R^*\left(\frac{d^2R^*}{d\theta^2} - R^*\right) - 2\left(\frac{dR^*}{d\theta}\right)^2}{\left[R^{*2} + \left(\frac{dR^*}{d\theta}\right)^2\right]^{3/2}} + \frac{\frac{\cot\theta}{r^*}\frac{dR^*}{d\theta} - 1}{\left[R^{*2} + \left(\frac{dR^*}{d\theta}\right)^2\right]^{1/2}} \tag{19}$$

Inviscid-Flow Solution Procedure. The solution of Laplace's equation in spherical coordinates is

$$\phi^*(r^*, \theta) = \sum_{n=0}^{\infty} A_{2n} r^{*2n} P_{2n}(\cos\theta) \tag{20}$$

where $P_{2n}(\cos\theta)$ is the Legendre function of $2n$ order. The Legendre function automatically satisfies the boundary condition (Eq. (7)) along the target and the axis of symmetry.

The coefficients A_{2n} cannot be determined by conventional

Downloaded 29 Jun 2009 to 18.80.1.33. Redistribution subject to ASME license or copyright; see http://www.asme.org/terms/Terms_Use.cfm

orthogonal-function methods. If the jet boundary can be located, we may pursue the problem using a modification of an alternative method due to Shen (1962), as follows.

Assume $f_n(\theta)$ is an arbitrary continuous function of θ, and multiply both sides of the boundary conditions by f_n. Substitute ϕ^* into the equations and integrate along the boundaries to obtain a set of nonlinear algebraic equations. By solving the set of algebraic equations, the coefficients A_{2n} can be calculated. Initially, the location of the jet's free boundary is both unknown and unlikely to coincide with a coordinate line. To proceed, we may assume a jet free boundary and integrate the equations along this assumed boundary; then we may correct the previous boundary and repeat the computation until the solution converges, satisfying both Eq. (14) and the boundary conditions (Eqs. (15)–(19)). Shen (1962) also suggested an iteration scheme for use with this method, but he did not carry it out.

The principal difficulty with Shen's iteration scheme was the lack of a method of successively correcting the free-boundary shape. We suggest an alternative method to locate the free boundary, as represented by the function $R^* = R^*(\theta)$. The constraint on the free surface is a flux condition that the total flow rate over every jet cross section must be the same. Specifically, for any θ,

$$\int_0^{R^*(\theta)} 2\pi \frac{d\phi^*}{d\theta} dr^* = Q^* \tag{21}$$

or, equivalently, for any R^*,

$$\int_0^{\theta(R^*)} 2\pi \frac{d\phi^*}{dr^*} R^* d\theta = Q^* \tag{22}$$

We integrate the total flow rate over a cross section. If the flow rate is larger than Q^*, we pull in the free boundary (Fig. 2). If the flow rate is smaller than Q^*, we push out the free boundary. Then, the correction function for Eq. (21) is

$$R^{*(n+1)}(\theta) = R^{*(n)}(\theta)\left[1+\beta\left(Q^* - \int_0^{R^{*(n)}(\theta)} 2\pi \frac{d\phi^*}{d\theta} dr^*\right)\frac{1}{Q^*}\right] \tag{23}$$

where β is a relaxation factor. The convergence of the iteration strongly depends on the value of β. In the present computation, β was chosen between 0.03 to 0.2. Similarly, for Eq. (22)

$$\theta^{(n+1)}(R^*) = \theta^{(n)}(R^*)\left[1+\beta\left(Q^* - \int_0^{\theta^{(n)}(R^*)} 2\pi R^* \frac{d\phi^*}{dr^*} d\theta\right)\frac{1}{Q^*}\right] \tag{24}$$

In the computation, discrete points on the free surface are chosen to be corrected by the above two equations. For points near the inlet and the outlet Eq. (24) is used; for the other points Eq. (23) is used, to achieve better convergence. The points that represent the shape of the free surface then are fitted to the following equation:

$$R^*(\theta) = A_o + \sum_{n=1}^{3} \frac{B_n}{(\theta - A_1)^n} + \sum_{n=1}^{3} \frac{C_n}{(A_2 - \theta)^n} \tag{25}$$

where A_0, A_1, A_2, B_n, C_n are adjustable constants. The accuracy of the curve fit is within ± 0.2 percent. This fitted equation is substituted back into the original equations to calculate a new set of coefficients of A_{2n}. In principle, it is not necessary to curve fit the points; the equation could be discretized instead. However, curve fitting simplifies the calculation significantly.

Boundary Layer Solution. For the boundary layer, cylindrical coordinates are more convenient than spherical coordinates, since the boundary layer is very thin and no singularity arises as for the free surface. The basic equations for axisymmetric flow are

$$\frac{\partial(ur)}{\partial r} + \frac{\partial(vr)}{\partial y} = 0 \tag{26}$$

$$u\frac{\partial \mathbf{v}}{\partial r} + v\frac{\partial \mathbf{v}}{\partial y} = -\frac{1}{\rho}\nabla p + \nu\nabla^2\mathbf{v} \tag{27}$$

with the energy equation

$$u\frac{\partial T}{\partial r} + v\frac{\partial T}{\partial y} = \alpha\nabla^2 T \tag{28}$$

In these equations, r represents the radial distance from the stagnation point and y the vertical distance from the target plane (White, 1991).

The velocity just outside the boundary layer can be obtained from Eq. (20)

$$U(r) = \sum_{n=0}^{\infty} 2nA_{2n} r^{2n-1} P_{2n}(\cos(\theta = \pi/4)) \tag{29}$$

Should be theta/2

Very close to the stagnation point only the first term in the above equation need be considered. The solution of the boundary layer equations can be obtained using a standard similarity transformation, from which the Nusselt number at the stagnation point is obtained as:

$$\mathrm{Nu}_d = G(\mathrm{Pr})\mathrm{Re}_d^{1/2}\sqrt{2\frac{d}{u_f}\frac{\partial U}{\partial r}} \tag{30}$$

where (White, 1974)

$$G(\mathrm{Pr}) \approx \begin{cases} \dfrac{\sqrt{2\,\mathrm{Pr}/\pi}}{1+0.804552\sqrt{2\mathrm{Pr}/\pi}} & \mathrm{Pr} \le 0.15 \\ 0.53898\,\mathrm{Pr}^{0.4} & 0.15 < \mathrm{Pr} < 3.0 \\ 0.60105\,\mathrm{Pr}^{1/3} - 0.050848 & \mathrm{Pr} \le 3.0 \end{cases} \tag{31}$$

Pr > 3

The boundary condition can be either uniform wall temperature or uniform wall heat flux, since the stagnation-point boundary layer thickness is independent of r. The effect of the Weber number, or surface tension, on Nusselt number is implicit in the above equation through its effect on the dimensionless velocity gradient.

4 Results

Validation of the flow-field solution is based on a comparison to existing results for infinite Weber number (Schach, 1935). The essential contribution of the flow field solution to the subsequent stagnation-point heat transfer analysis is the streamwise velocity gradient that enters the Nusselt number

$$B = 2\frac{d}{u_f}\frac{dU}{dr} \tag{32}$$

For the present solutions, B is 1.832 for infinite Weber number. This value differs from Schach's value of 1.76 by only 4 percent, corresponding to a difference of about 2 percent in Nusselt number. While both the present solution and Schach's result are approximate, the good agreement between the two results lends a measure of confidence to the present procedure. An experimental comparison is described below.

Calculated Inviscid Flow Field and Velocity Profiles. Figure 3 shows the free-surface shape and nondimensional inviscid velocity distribution, v/u_f, for infinite Weber number. In the plane of the axis of symmetry, the radius of curvature of the free surface is smaller than the jet radius. For an axisymmetric jet, the free surface begins to deflect much closer to the target than for a planar jet.

Free-surface deflection is caused by the increased pressure near the stagnation point. The above characteristics are also seen in Fig. 4, which shows the calculated nondimensional pressure distribution, p/P_0. The pressure is a maximum at the

Downloaded 29 Jun 2009 to 18.80.1.33. Redistribution subject to ASME license or copyright; see http://www.asme.org/terms/Terms_Use.cfm

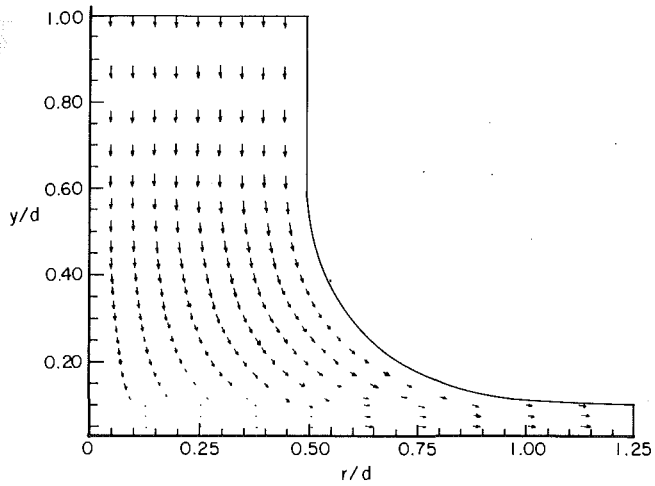

Fig. 3 The inviscid velocity field, v^*, for $We_d \to \infty$ from the potential-flow solution

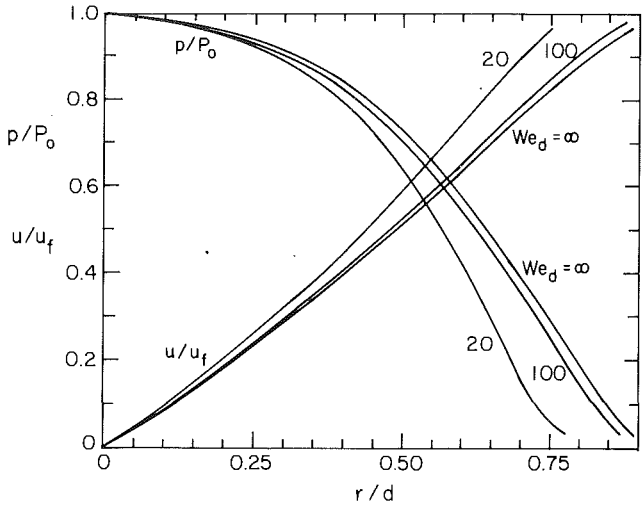

Fig. 6 Velocity and pressure variation along the target plate ($y/d = 0$) for several values of Weber number and inviscid flow

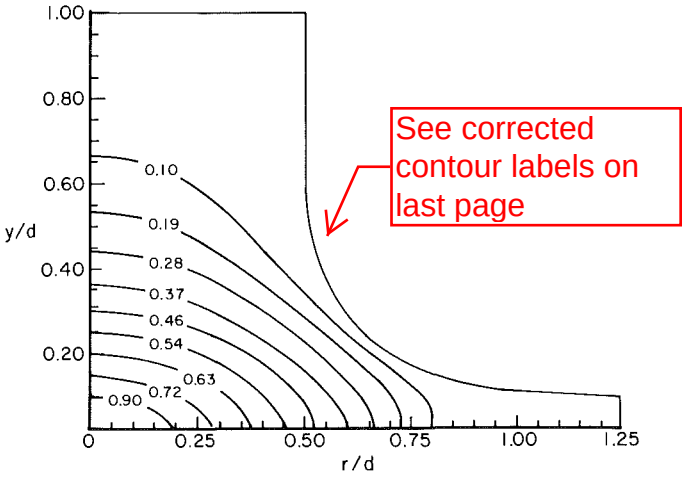

Fig. 4 The inviscid pressure distribution, p/P_0, as $We_d \to \infty$

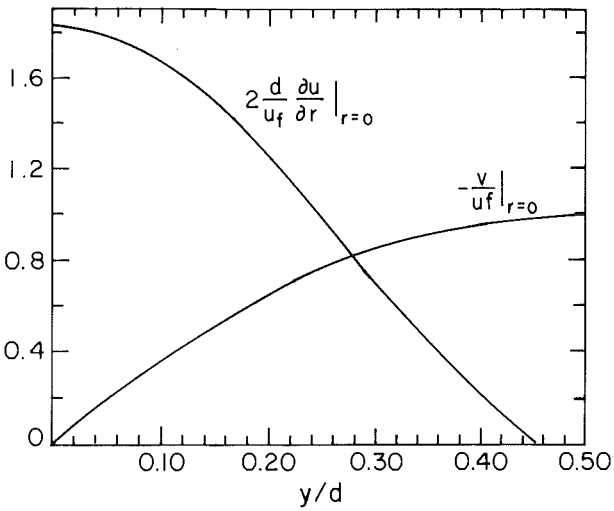

Fig. 7 Vertical profiles of downward velocity and radial velocity-gradient along jet centerline for inviscid flow ($We_d \to \infty$)

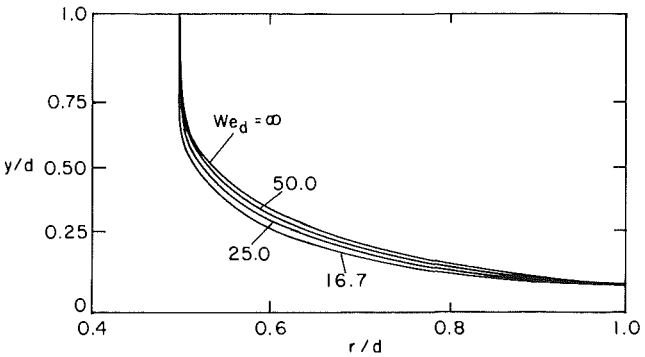

Fig. 5 The free-surface shape for several values of Weber number and inviscid flow

stagnation point and decreases steadily with increasing radius. In the region $r < 0.25d$, the nondimensional pressure is larger than 0.75; beyond $r/d = 0.8$, the pressure is less than 10 percent of the stagnation pressure.

The Role of Weber Number. Figure 5 shows the calculated free-surface shape as a function of Weber number. The free-surface deflection is progressively reduced as Weber number decreases. This happens because surface tension provides an additional restoring force, which balances the higher pressure near the stagnation region.

A lower bound on the Weber number is set by surface-tension choking of the nozzle. Lienhard and Lienhard (1984) showed that flow from a circular orifice will choke when

$$We_{d_o} = \frac{\rho u_f^2 d_o}{\sigma} \approx 8 \tag{33}$$

where the orifice diameter is d_o. Under these conditions, the surface-tension force prevents a steady flow from the upstream plenum.

Figure 6 shows the velocity and pressure variation along the target plate at different Weber numbers. The smaller the Weber number, the faster the velocity grows with radius and the quicker the pressure drops along the plate. Because the surface curvature changes from concave (along the incoming jet) to almost flat (in the far field), surface tension pressure decreases radially and produces a net increase in the momentum of the outflowing liquid. Thus, the downstream velocity tends toward the ideal-jet velocity, $\sqrt{2P_0/\rho}$, which is greater than the incoming velocity u_f. The vertical velocity distribution is shown in Fig. 7.

A previous paper (Liu et al., 1991) estimated from boundary layer growth ideas that the stagnation zone is confined to the

Downloaded 29 Jun 2009 to 18.80.1.33. Redistribution subject to ASME license or copyright; see http://www.asme.org/terms/Terms_Use.cfm

Miyazaki: add row 0.393, planar, uniform, infinity, infinity

B is based on half-width for planar jets and on bulk velocity for nonuniform jets

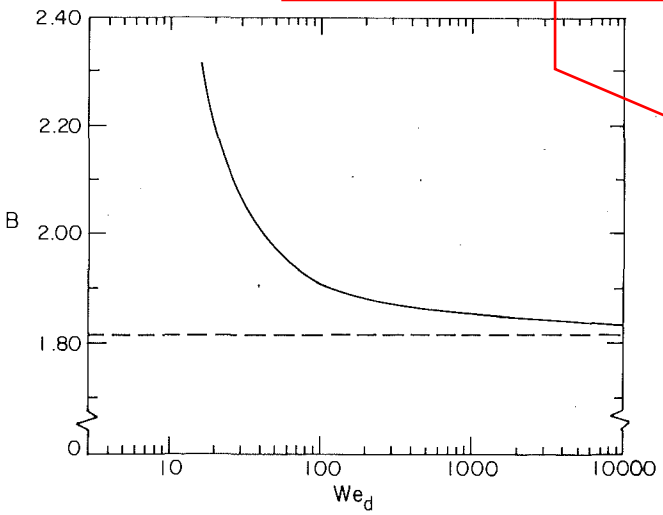

Fig. 8 Effect of Weber number on the free-stream (inviscid) stagnation-point velocity gradient, $B = 2(d/u_f)(\partial U/\partial r)$

Table 1 Velocity gradients at the stagnation point during laminar jet impingement: $B/2 = (d/u_f)(\partial U/\partial r)$; l is either the height of the inviscid-flow computational-domain or the experimental jet's length

Investigators	$B/2$	jet type	inlet velocity profile	l/d	We_d
Miyazaki and Silberman (1972)	~~0.951~~	planar	uniform	0.5	∞
	~~0.457~~	planar	uniform	1.5	∞
Sparrow and Lee (1975)	~~0.964~~	planar	uniform	0.5	∞
	~~0.445~~	planar	uniform	1.5	∞
	~~0.393~~	~~planar~~	~~uniform~~	~~∞~~	~~∞~~
	1.74	planar	parabolic	0.25	∞
	1.51	planar	parabolic	1.5	∞
Scholtz and Trass (1970)	~~3.76~~	circular	parabolic	~~1.0~~	∞
	~~0.731~~	~~circular~~	~~uniform~~	~~1.0~~	~~∞~~
Schach (1935)	0.88	circular	uniform	1.5	∞
Shen (1962)	0.743	circular	uniform	1.5	∞
Strand (1964)	~~0.958~~	circular	uniform	1.0	∞
Present computations	0.916	circular	uniform	1.0	∞
	0.981	circular	uniform	1.0	50
	1.06	circular	uniform	1.0	25
	1.16	circular	uniform	1.0	16.7
Present data	0.77	circular	uniform	> 6	> 2100

Table 2 Axisymmetric stagnation-point Nusselt number expressions for various investigations

Investigators	Nu_d	Velocity gradient & initial distribution
Scholtz and Trass (1970)	$0.727\,Re_d^{1/2}Pr^{0.361}$ $1<Pr<10$, $l/d=1.0$	Strand (1964) uniform laminar
Scholtz and Trass (1970)	$1.648\,Re_d^{1/2}Pr^{0.361}$ $1<Pr<10$, $l/d=0.5$	Inviscid vortex eqn., parabolic
Nakoryakov *et al.* (1978)	$0.753\,Re_d^{1/2}Pr^{1/3}$	Schach (1935) uniform laminar
Liu *et al.* (1991) Eqn. 30	$0.797\,Re_d^{1/2}Pr^{1/3}$ $Pr>3$, $l/d>1.5$	Schach (1935) uniform laminar
Eqn. 30	$0.813\,Re_d^{1/2}Pr^{1/3}$ $Pr>3$, $l/d=1$	Present $(We_d \to \infty)$
Eqn. 30	$0.832\,Re_d^{1/2}Pr^{1/3}$ $Pr>3$, $l/d=1.5$	Strand (1964) $(We_d \to \infty)$
Eqn. 30	$0.733\,Re_d^{1/2}Pr^{1/3}$ $Pr>3$, $l/d=1.5$	Shen (1962) $(We_d \to \infty)$
Lienhard *et al.* (1991)	$1.24\,Re_d^{1/2}Pr^{1/3}$ $Pr>3$, $l/d>1.5$	Correlation, turbulent/splattering
Stevens and Webb (1991)	$2.67\,Re_d^{0.567}Pr^{0.4}(l/d)^{-0.0336}(u_f/d)^{-0.237}$	Correlation, turbulent

region $r/d \le 0.787$. Figure 6 shows that the linear rise of velocity expected for true stagnation-point flow occurs only for $r/d < 0.35$, although it may provide a useful approximation to r/d as large as 0.75.

Figure 8 and Table 1 show the effect of Weber number on the velocity gradient at the stagnation point. The dimensionless gradient, B, at the stagnation point is higher for smaller values of Weber number. The increase is related to both the decrease in free-surface deflection (Fig. 5) and the increase of the downstream speed above the incoming liquid speed (Fig. 6). As the Weber number decreases from infinity to 16.7, the dimensionless velocity gradient increases by 26 percent. Since the Nusselt number is proportional to the square root of the velocity gradient, the Nusselt number goes up by about 13 percent. For common cooling applications with water, the Weber number is usually more than several hundred, and Weber number effects will be negligible. For low-velocity small-diameter jets, however, such effects may have some importance.

Table 2 shows the Nusselt number formulae obtained from Eq. (30) when the values of B from this or other investigations are employed or when different expressions for $G(\mathrm{Pr})$ are used. The theoretical results may be compared to experimental data available for high Weber numbers. Experiments with uniform velocity profile, laminar jets for $2100 < We_d < 34{,}000$ and high Reynolds numbers are represented by

$$Nu_d = 0.745\,Re_d^{1/2}\,Pr^{1/3} \tag{34}$$

to an accuracy of about ± 5 percent (for details, see Liu, 1992; Liu et al., 1991, present some related data). In general, the predictions are in good agreement with the data.

Two comments should be made in regard to turbulent liquid jets. First, because the Reynolds number is greater than 2400 for most turbulent jets, the Weber number is usually large, as is seen from the following:

$$We_d = \left(\frac{\rho u_f d}{\mu}\right)^2 \frac{\mu^2}{\rho\sigma d} = Re_d^2 \frac{\mu^2}{\rho\sigma d} \tag{35}$$

Thus, unless jet diameter is very small, direct stagnation-point surface-tension effects can be neglected for turbulent jets.

Second, turbulence may increase the Nusselt number at the stagnation point by disrupting the already thin boundary layer there. This effect has been experimentally observed by comparing nearly-uniform-profile turbulent and laminar liquid jets (Lienhard et al., 1992), and is well documented in submerged flows and submerged jets (Kestin, 1966; Mehendale et al., 1991; Simmons et al., 1990). The laminar formulae developed above are not recommended for turbulent jets.

5 Conclusions

The influence of surface tension on stagnation-point heat transfer beneath an impinging liquid jet has been analytically studied. The results include the zero-surface-tension (high Weber number) case as a limit. Various past results for the stagnation-point Nusselt number are also summarized.

- Surface tension affects the stagnation-point velocity gradient and Nusselt number for We_d less than about 100. The increase in Nusselt number is about 13 percent at a Weber number of 16.7. For most industrial cooling applications, however, We_d is too large for this effect to be of significance.
- The dimensionless stagnation-point velocity gradient obtained for $We_d \to \infty$ is $B = 1.832$, in good agreement with the results of Schach (1935) and others.
- Stagnation-point Nusselt number formulae for this and previous investigations are summarized in Table 2. Those results include both laminar and turbulent jets with both uniform and nonuniform velocity profiles; most have experimental validation. For laminar jets, the results differ principally in the method of correlating Prandtl number effects; more data are needed at very high and very low Prandtl number. For high Weber number, uniform, laminar jets, and experimental data are well represented by $Nu_d = 0.745\,Re_d^{1/2}Pr^{1/3}$, which is within the range of the various predictions.

Downloaded 29 Jun 2009 to 18.80.1.33. Redistribution subject to ASME license or copyright; see http://www.asme.org/terms/Terms_Use.cfm

Acknowledgments

This work was supported by the A. P. Sloan Foundation and by the National Science Foundation under grant No. CBT-8858288.

References

Crank, J., 1984, *Free and Moving Boundary Problems*, Clarendon Press, Oxford, United Kingdom.

Davies, J. T., and Makepeace, 1978, "Measurement of the Surface Ages of Water Jets," *AIChE Journal*, Vol. 24, No. 3, pp. 524–530.

Duda, J. L., and Vrentas, J. S., 1967, "Fluid Mechanics in Laminar Liquid Jets," *Chem. Eng. Sci.*, Vol. 22, p. 866.

Kestin, J., 1966, "The Effect of Free-Stream Turbulence on Heat Transfer Rates," *Adv. Heat Transfer*, Vol. 3, pp. 1–32.

Lienhard, J. H., V, and Lienhard, J. H., 1984, "Velocity Coefficients for Free Jets From Sharp-Edged Orifices," ASME *Journal of Fluid Engineering*, Vol. 106, pp. 13–17.

Lienhard, J. H., V, Liu, X., and Gabour, L. A., 1992, "Splattering and Heat Transfer During Impingement of a Turbulent Liquid Jet," ASME JOURNAL OF HEAT TRANSFER, Vol. 114, pp. 362–372.

Liu, X., Lienhard, J. H., V, and Lombara, J. S., 1991, "Convective Heat Transfer by Impingement of Circular Liquid Jets," ASME JOURNAL OF HEAT TRANSFER, Vol. 113, pp. 571–582.

Liu, X., 1992, "Liquid Jet Impingement Heat Transfer and Its Potential Applications at Extremely High Heat Fluxes," Doctoral Thesis in Mechanical Engineering, MIT, Cambridge, MA.

Mehendale, A. B., Han, J. C., and Ou, S., 1991, "Influence of High Mainstream Turbulence on Leading Edge Heat Transfer," ASME JOURNAL OF HEAT TRANSFER, Vol. 113, pp. 843–850.

Miyazaki, H., and Silberman, E., 1972, "Flow and Heat Transfer on a Flat Plate Normal to a Two-Dimensional Laminar Jet Issuing From a Nozzle of Finite Height," *Int. J. Heat Mass Transfer*, Vol. 15, pp. 2097–2107.

Nakaryakov, V. E., Pokusaev, B. G., and Troyan, E. N., 1978, "Impingement of an Axisymmetric Liquid Jet on a Barrier," *Int. J. Heat Mass Transfer*, Vol. 21, No. 9, pp. 1175–1184.

Schach, W., 1935, "Umlenkung eines kreisförmigen Flussigkeitsstrahles an einer ebenen Platte senkrecht zur Strömungsrichtung," *Ing.-Arch.*, Vol. 6, pp. 51–59.

Schlichting, H., 1979, *Boundary Layer Theory*, 7th ed., McGraw-Hill, New York.

Scholtz, M. T., and Trass, O., 1970, "Mass Transfer in a Nonuniform Impinging Jet," *AIChE Journal*, pp. 82–96.

Scriven, L. E., and Pigford, R. L., 1959, "Fluid Dynamics and Diffusion Calculations for Laminar Liquid Jets," *AIChE Journal*, Vol. 5, p. 397.

Shen, Y. C., 1962, "Theoretical Analysis of Jet-Ground Plane Interaction," IAS Paper No. 62–144.

Simmons, S. G., Hager, J. M., and Diller, T. E., 1990, "Simultaneous Measurements of Time-Resolved Surface Heat Flux and Freestream Turbulence at a Stagnation Point," *Heat Transfer 1990*, Proc. Ninth Intl. Heat Transfer Conf., Jerusalem, Vol. 2, pp. 375–380.

Sparrow, E. M., and Lee, L., 1975, "Analysis of Flow Field and Impingement Heat/Mass Transfer Due to a Nonuniform Slot Jet," ASME JOURNAL OF HEAT TRANSFER, Vol. 97, pp. 191–197.

Stevens, J., and Webb, B. W., 1991, "Local Heat Transfer Coefficients Under an Axisymmetric Single-Phase Liquid Jet," ASME JOURNAL OF HEAT TRANSFER, Vol. 113, pp. 71–78.

Strand, T., 1964, "On the Theory of Normal Ground Impingement of Axisymmetric Jets in Inviscid Incompressible Flow," AIAA Paper No. 64–424.

White, F. M., 1974, *Viscous Fluid Flow*, McGraw-Hill, New York, p. 183.

White, F. M., 1991, *Viscous Fluid Flow*, 2nd ed., McGraw-Hill, New York, pp. 159–162.

Downloaded 29 Jun 2009 to 18.80.1.33. Redistribution subject to ASME license or copyright; see http://www.asme.org/terms/Terms_Use.cfm

Errata for
"Stagnation-Point Heat Transfer During Impingement of Laminar Liquid Jets: Analysis with Surface Tension Effects "
by Liu, Gabour, and Lienhard
Journal of Heat Transfer, **Vol. 115, pp.99–105, Feb. 1993**

1. Equation 29: replace "$\theta/4$" with "$\theta/2$".

2. Equation 31: the last line applies for $\mathrm{Pr} \geq 3$ not ≤ 3.

3. Figure 4: the levels of pressure are mislabeled. The correct labels are:

Value on Fig.	Correct Value
0.10	0.19
0.19	0.34
0.28	0.48
0.37	0.60
0.46	0.71
0.54	0.79
0.63	0.86
0.72	0.92
0.90	0.96

4. Page 103, line 2: replace "$r < 0.25d$" with "$r < 0.5d$".

5. Page 103, line 3: replace "less than 10%" with "less than 20%".

6. Table 1: Corrections to a few lines are as shown. Also note that B is based on half-width for the planar jets and on bulk velocity for nonuniform jets.

Investigators	$B/2$	jet type	inlet velocity profile	l/d	We_d
Miyazaki and Silberman (1972)	*0.964*	planar	uniform	0.5	∞
	0.445	planar	uniform	1.5	∞
	0.393	*planar*	*uniform*	∞	∞
Sparrow and Lee (1975)	*0.951*	planar	uniform	0.5	∞
	0.457	planar	uniform	1.5	∞
	omit	planar	uniform		∞
Scholtz and Trass (1970)	*4.69*	circular	parabolic	*0.05–0.5*	∞
	omit		uniform		
Strand (1964)	*0.903*	circular	uniform	1.0	∞